marine drugs

MDPI

Article

Structure Elucidation, Biosynthetic Gene Cluster Distribution, and Biological Activities of Ketomemicin Analogs in *Salinispora*

Gabriel Castro-Falcón [1,*,†], Dulce G. Guillén-Matus [1,†], Elany Barbosa Da Silva [2], Wentao Guo [3], Alicia Ross [3], Mateus Sá Magalhães Serafim [2,4], Thaís Helena Maciel Fernandes [2], Dean J. Tantillo [3], Anthony J. O'Donoghue [2] and Paul R. Jensen [1]

[1] Center for Marine Biotechnology and Biomedicine, Scripps Institution of Oceanography, University of California San Diego, La Jolla, CA 93093, USA
[2] Skaggs School of Pharmacy and Pharmaceutical Sciences, Center for Discovery and Innovation in Parasitic Diseases, University of California San Diego, La Jolla, CA 92093, USA
[3] Department of Chemistry, University of California Davis, Davis, CA 95616, USA
[4] Department of Microbiology, Institute of Biological Sciences, Federal University of Minas Gerais, Belo Horizonte 31270901, MG, Brazil
* Correspondence: g6castro@ucsd.edu
† These authors contributed equally to this work.

Abstract: Pseudopeptides are attractive agents for protease inhibition due to their structural similarities to the natural substrates of these enzymes, as well as their enhanced stability and resistance to enzymatic degradation. We report three new ketomemicin pseudopeptides (**1**–**3**) from extracts of the marine actinomycete *Salinispora pacifica* strain CNY-498. Their constitution and relative configuration were elucidated using NMR, mass spectrometry, and quantum chemical calculations. Using GNPS molecular networking and publicly available *Salinispora* LCMS datasets, five additional ketomemicin analogs (**4**–**8**) were identified with ketomemicin production detected broadly across *Salinispora* species. The ketomemicin biosynthetic gene cluster (*ktm*) is highly conserved in *Salinispora*, occurring in 79 of 118 public genome sequences, including eight of the nine named species. Outside *Salinispora*, *ktm* homologs were detected in various genera of the phylum Actinomycetota that might encode novel ketomemicin analogs. Ketomemicins **1**–**3** were tested against a panel of eleven proteases, with **2** displaying moderate inhibitory activity. This study describes the first report of ketomemicin production by *Salinispora* cultures, the distribution of the corresponding biosynthetic gene cluster, and the protease inhibitory activity of new ketomemicin derivatives.

Keywords: natural products; *Salinispora*; ketomemicins; pseudopeptides

Academic Editor: Huayue Li

Received: 21 February 2025
Revised: 8 March 2025
Accepted: 11 March 2025
Published: 14 March 2025

Citation: Castro-Falcón, G.; Guillén-Matus, D.G.; Silva, E.B.D.; Guo, W.; Ross, A.; Sá Magalhães Serafim, M.; Fernandes, T.H.M.; Tantillo, D.J.; O'Donoghue, A.J.; Jensen, P.R. Structure Elucidation, Biosynthetic Gene Cluster Distribution, and Biological Activities of Ketomemicin Analogs in *Salinispora*. *Mar. Drugs* **2025**, *23*, 126. https://doi.org/10.3390/md23030126

1. Introduction

The pseudopeptide natural products ketomemicin A, B1–B6, and C were previously discovered following heterologous expression of biosynthetic gene clusters (BGCs) from *Micromonospora* sp. ATCC-39149, *Streptomyces mobaraensis* NBRC 13819, and *Salinispora tropica* CNB-440, respectively (Figure 1) [1]. The six-gene BGCs, named *ktm*, encode an aldolase (*ktmA*), a pyridoxal 5′-phosphate (PLP)-dependent amino acid C-acyltransferase (*ktmB*), a dehydratase (*ktmC*), an ATP-Grasp peptide ligase (*ktmD*), an amidinotransferase (*ktmE*), and a dehydrogenase (*ktmF*), and are thus independent of the more traditional ribosomal and non-ribosomal peptide synthetase (NRPS) pathways of peptide natural product biosynthesis [1–3]. Ketomemicins have not been previously reported from *Salinispora*

strains [4] nor were they detected in culture extracts of *S. tropica* CNB-440 [1], suggesting the BGC remained silent under the laboratory growth conditions employed.

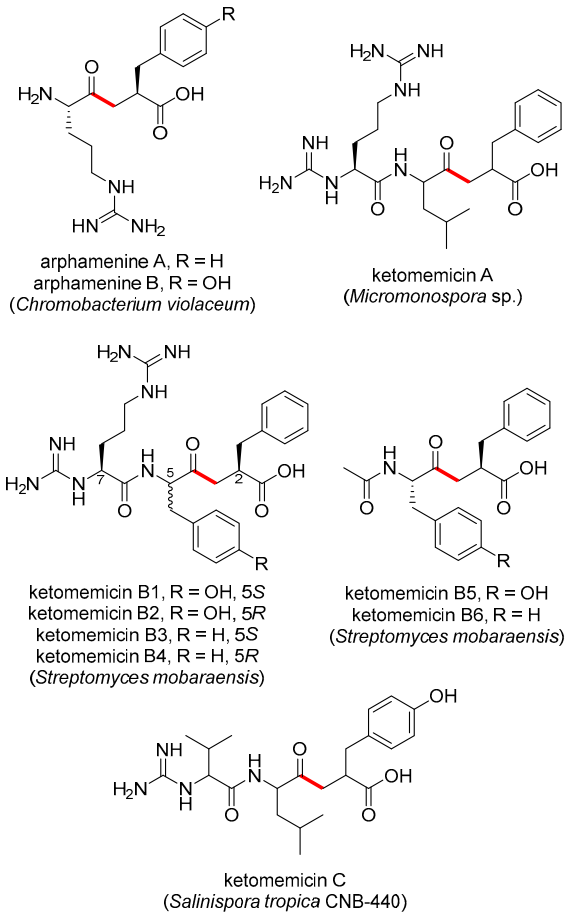

Figure 1. Previously reported ketomethylene-containing pseudopeptide natural products, arphamenines and ketomemicins. The ketomethylene bond in each structure is shown in red. Producing organisms are shown in parentheses.

The natural products arphamenine A and B are structurally similar to the ketomemicins. They were discovered from the Gram-negative bacterium *Chromobacterium violaceum* due to their ability to inhibit the mammalian protease aminopeptidase B [5,6]. Both ketomemicins and arphamenines contain amino acid residues typical of peptides but are considered pseudopeptides due to the presence of a ketomethylene bond in lieu of a typical peptide bond. Although ketomemicins and arphamenines are the only known naturally occurring ketomethylene-containing pseudopeptides, synthetic peptides with similar structures have been developed as protease inhibitors [7]. Interestingly, the isosteric replacement of a peptide bond to a ketomethylene bond may be an evolved strategy of natural product protease inhibitors [8]. However, we are unaware of any prior data describing the effects of the ketomemicins on protease activity.

In this work, we report the structures, relative configuration, and protease inhibitory activities of three novel ketomemicins (**1**–**3**) obtained from culture extracts of *Salinispora pacifica* CNY-498. We evaluated the production of ketomemicin analogs across *Salinispora* metabolomic datasets and assessed the diversity and distribution of the *ktm* BGC in the genus *Salinispora* and, more broadly, in the phylum Actinomycetota to show that additional diversity likely remains to be discovered within this unusual compound class.

2. Results and Discussion

2.1. Isolation and Structure Elucidation of Ketomemicins

HPLC-MS screening of *Salinispora* culture extracts revealed three compounds produced by *S. pacifica* CNY-498 that were suggestive of a new series of natural products. To obtain enough of these compounds for NMR structure elucidation and biological testing, strain CNY-498 was grown in 18 × 1 L cultures in A1FB medium with the addition of the adsorbent resin XAD-7 at day 8. The organic eluent from the collected resin and cells was subjected to C_{18} flash chromatography using a six-step solvent gradient of H_2O and MeCN, resulting in a fraction enriched in the three target compounds. This fraction was subjected to preparative HPLC to yield 0.8, 0.7, and 0.5 mg of compounds **1**–**3**, respectively. Structure elucidation using HRMS and NMR spectroscopic analysis revealed that all three compounds were new derivatives of the natural product ketomemicin C, herein named according to their respective molecular mass as ketomemicin C-418 (**1**), ketomemicin C-432A (**2**), and ketomemicin C-432B (**3**) (Figure 2 and Supplementary Figures S1–S15).

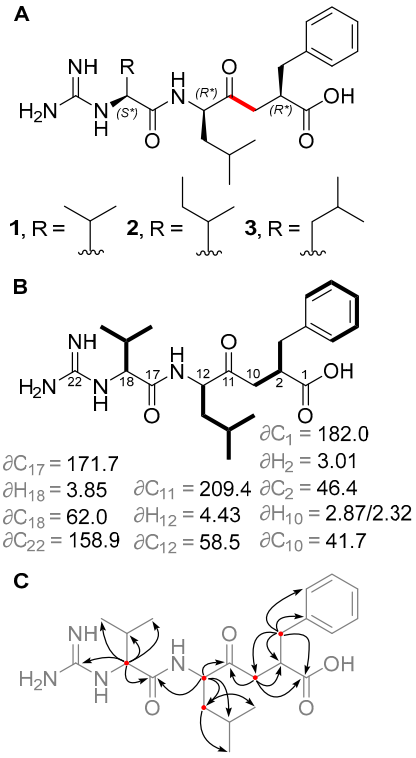

Figure 2. (**A**) Structures of new ketomemicins (**1**–**3**) isolated in this work (ketomethylene bond in red). (**B**) ^{1}H and ^{13}C NMR chemical shifts (in ppm) of backbone atoms and ^{1}H–^{1}H COSY correlations (bolded bonds) observed for **1**. (**C**) Key HMBC correlations observed for **1** represented as arrows from ^{1}H to ^{13}C atoms.

Ketomemicin C-418 (**1**), isolated as a thin white film, was analyzed by HRMS to give the molecular formula $C_{22}H_{34}N_4O_4$ (observed 419.2650 m/z $[M + H]^+$, calculated 419.2653, −0.67 ppm error). In CD_3OD, the ^{1}H NMR spectrum indicated five aromatic protons (δH 7.16, 7.23, and 7.25 ppm), seven deshielded aliphatic protons (δH 2.32/2.87, 2.65/3.06, 3.01, 3.85, and 4.43 ppm), and 16 shielded aliphatic protons (δH 0.92–2.19 ppm), totaling 28 hydrocarbon protons. The remaining six protons exchanged with the deuterated NMR solvent and could not be detected. HSQC and HMBC spectra revealed all 22 carbons in **1**, including a ketone (δC 209.4 ppm), carboxylic acid (δC 182.0 ppm), amide (δC 171.7 ppm), carbonyl alpha-carbons (δC 41.7, 46.4, 58.5, 62.0 ppm), aromatic (δC, 126.9–141.5 ppm), guanidine (δC 158.9 ppm), and aliphatic carbons (δC 17.8–39.7 ppm). COSY and HMBC

spectra, respectively, showed four spin systems and their interconnectedness (Figure 2B,C). Compound **1** resembles the tripeptide Val-Leu-Phe but with a ketomethylene replacement (C_{10}–C_{11}) and a guanidine group at the N-terminal valine. Notably, in the ^{1}H NMR spectrum, one of the ketomethylene protons (δ 2.87 ppm) exhibited a relatively diminished peak area due to partial exchange with deuterium, attributed to its acidity.

Ketomemicin C-432A (**2**) and ketomemicin C-432B (**3**) were also isolated as thin white films. Their HRMS analysis indicated these were isomers with the molecular formula $C_{23}H_{36}N_4O_4$ (calculated 433.2810 for M + H^+) due to observed values of 433.2820 and 433.2824 *m*/*z* (2.31 and 3.00 ppm error, respectively). The NMR spectra for both **2** and **3** closely resembled that of **1**, except for signals related to the N-terminal amino acid, which indicated the presence of an isoleucine in **2** and a leucine in **3**. While the MS^2 spectra of **2** and **3** were very similar, the spectrum of **2** exclusively displayed a small fragment ion at 69.1 *m*/*z* indicative of the isoleucine residue (Figures S5 and S10) [9].

The relative configuration of **1** was determined by comparing the experimental ^{1}H and ^{13}C NMR chemical shift values to those calculated for the four possible diastereomers of **1** (as the guanidinium-carboxylate zwitterion) using quantum chemical computations [10]. Distinguishing the correct diastereomer presented a substantial challenge due to the flexibility of the molecules and the quantity of polar groups they contain. For each diastereomer, conformational searching was conducted using xTB-CREST to identify low-energy conformers [11]. These low-energy conformers were then optimized using *Gaussian16* at the restricted B3LYP-D3(0)/6-31 + G(d,p) level of theory with an implicit solvation model for methanol (IEFPCM) [12–16]. NMR chemical shift calculations were then performed for the lowest energy conformers within a 3 kcal/mol energy window using mPW1PW91/6-311 + G(2d,p), with methanol as solvent [17,18]. The isotropic shielding values obtained from these calculations were converted to chemical shifts using scaling factors from the CHESHIRE dataset [10]. The computed chemical shifts of the conformers for each diastereomer were weighted and averaged based on their relative free energies at the IEFPCM(methanol)-B3LYP/6-31 + G(d,p) level using a script provided by Hoye and co-workers [19]. A comparison was made between the experimentally determined and the predicted chemical shifts of the candidate diastereomers. However, due to the similarity of the predicted chemical shifts for the four diastereomers, the conventional criteria of root-mean-square deviation (RMSD) and mean absolute error (MAE) were unable to provide a definitive assignment; all candidates exhibited a strong correlation between the experimental and computation NMR data, having only small deviations and no large outliers. Thus, a DP4+ analysis was conducted to obtain a more robust confidence analysis for the four diastereomers [20]. This analysis revealed that the (2R*, 12R*, 18S*) diastereomer was the best match to the experimental chemical shifts, with a computed probability of >92% when considering both ^{1}H and ^{13}C signals. Therefore, we consider this relative configuration to be the most probable (Tables S4–S7). The same relative configuration was assumed for **2** and **3** due to the almost identical NMR chemical shifts and specific optical rotation values of **1**–**3**. Unfortunately, we were unable to determine the absolute stereochemistry of these compounds. In this case, we did not pursue absolute determination using Marfey's method because hydrolysis of the peptide bond in **1**–**3** would result in products that are unreactive towards FDAA or difficult to synthesize for standard validation.

2.2. Diversity and Distribution of Ketomemicins in Salinispora

Using GNPS molecular networking [21], we queried for ketomemicin analogs with similar MS^2 spectra to **1**–**3** in published LC-MS/MS datasets from *Salinispora* spp. [22–24] This led to the identification of five ketomemicin analogs (**4**–**8**) in the Crüsemann et al. (2017) dataset [23], which includes organic extracts of 118 genome-sequenced *Salinispora*

strains grown on agar (Figure S16). The constitution of **4**–**8** could be putatively assigned by comparing their MS^2 spectra with that of **1**–**3** (Figure 3). While **6** is identical in constitution to the previously reported ketomemicin C (herein referred to as ketomemicin C-434) [1] and **7** was previously reported based on the analysis of MS data [2], **4**, **5**, and **8** are new compounds. Notably, the ketomethylene bond in all arphamenines and ketomemicins discovered to date is associated with a C-terminal phenylalanine- or tyrosine-derived residue.

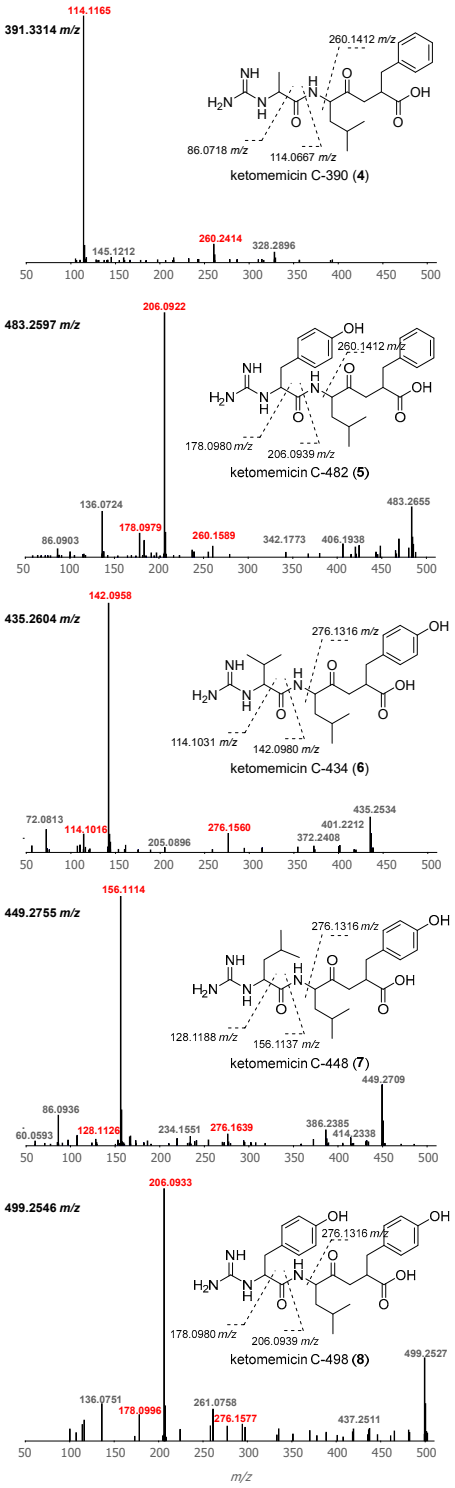

Figure 3. Structures and MS^2 spectra of ketomemicins **4**–**8**. Characteristic mass fragments (in red) putatively arise from the cleavage of bonds crossed with dashed lines. Precursor masses are shown for each spectrum (top-left).

We next analyzed for ketomemicins across the Crüsemann et al. (2017) dataset [23] using the "targeted feature detection" function within MZmine and the mass, retention time, and fragment ions as defining features for each metabolite [25]. From this analysis, we observed the production of **1**–**8** in 25 of 118 *Salinispora* strains (Table S4), corresponding to six of the nine currently described *Salinispora* species [26]. The vast majority of these strains (19/25) were *Salinispora tropica* and *Salinispora pacifica*. When mapped on a maximum-likelihood phylogeny generated using 2011 core genes from 118 *Salinispora* genomes [26], ketomemicin production was widely observed in *S. tropica* and more localized to specific clades within *S. pacifica* (Figure 4A). Furthermore, species-specific production patterns were observed as ketomemicins **6**–**8** with the C-terminal tyrosine-derived residue were mainly produced by *S. tropica* while ketomemicins **1**–**4** with the C-terminal phenylalanine-derived residue were mainly produced by the other *Salinispora* spp., in particular *S. pacifica* (Figure 4A and Table S4). Notably, only one of three *Salinispora mooreana* strains produced ketomemicins and it yielded the highest levels of **1**–**3** across the entire dataset, while *Salinispora arenicola* and *Salinispora oceanensis* showed low and infrequent production of **1**–**8** (observed in 3/61 and 1/13 strains, respectively). Compound **5** was only seen in one of two *Salinispora fenicalii* strains, while ketomemicin production (**1**–**8**) was not observed in *Salinispora cortesiana*, *Salinispora goodfellowii*, or *Salinispora vitiensis*. Together, these analyses reveal the broad yet inconsistent production of ketomemicins across the genus *Salinispora*.

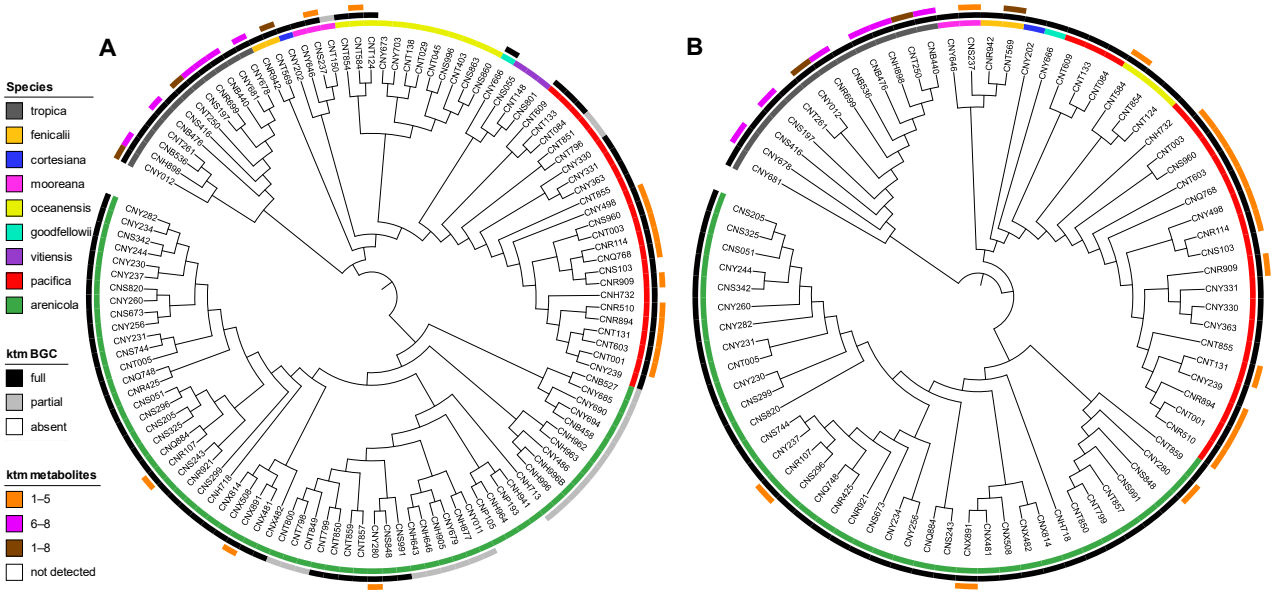

Figure 4. Phylogenetic relationships of ketomemicin production and the *ktm* BGC in *Salinispora*. (**A**) Phylogenomic tree of 118 *Salinispora* strains representing all nine currently described species (inner circle), distribution of the *ktm* BGC (middle circle), and observed production of ketomemicins with C-terminal phenylalanine-derived residue (**1**–**5**), C-terminal tyrosine-derived residue (**6**–**8**), or both (**1**–**8**) (outer circle). (**B**) Phylogeny (bootstrap value of 1000) of the complete *ktm* BGC observed in 79 *Salinispora* strains.

2.3. Diversity and Distribution of ktm in Salinispora spp. and Actinomycetota

Using AntiSMASH [27], we detected high percent similarity homologs of all six ketomemicin biosynthetic genes (*ktmA-F*) reported from *Streptomyces mobaraensis* NBRC 13,819 [1] in *S. pacifica* CNY-498. Using the *S. pacifica* BGC as input, we queried 118 *Salinispora* genomes using Cblaster [28] and identified all six *ktm* genes (≥87% identity and 97% coverage) in 79 *Salinispora* strains spanning eight of the nine species (Figure 4A and Figure S17). Interestingly, we also detected incomplete or partial *ktm* clusters containing two to five *ktm* genes (≥87% identity and 54% coverage) in 23 *Salinispora* genomes (20 *S. arenicola*,

2 *S. pacifica*, and 1 *S. mooreana*). These partial gene clusters were not on contig edges and thus do not appear to be sequencing artifacts. Similar observations of incomplete BGCs have been made for the desferrioxamine BGC (*des*) in *Salinispora* [29]. Using Clinker [30], we observed high gene synteny among the *ktm* BGCs, although species-specific differences in the flanking genes suggest that they may occur in different genomic environments (Figures 5 and S17), as reported for other *Salinispora* BGCs [31]. A *ktm* BGC phylogeny generated using all six genes from the 79 *Salinispora* genomes was highly congruent with the phylogenomic tree (Figure 4B), suggesting that *ktm* was present in the *Salinispora* common ancestor and has largely been passed down through vertical transmission. One exception is observed for *S. oceanensis* strains, which appear to have acquired the BGC from *S. pacifica* based on their position within the *S. pacifica* clade. When examining the relationships between the *ktm* BGC and ketomemicin production (Figure 4A), compounds were only detected in 25 (31.6%) of the 79 strains with the six gene operon. In *S. arenicola*, they were only detected in 3 (8.1%) of 37 strains. It remains unclear if the BGCs that could not be linked to compound production are non-functional or are under different regulatory control. There was no evidence of the former based on comparative sequence analysis. As expected, ketomemicins were not detected in any of the strains with a partial *ktm* BGC.

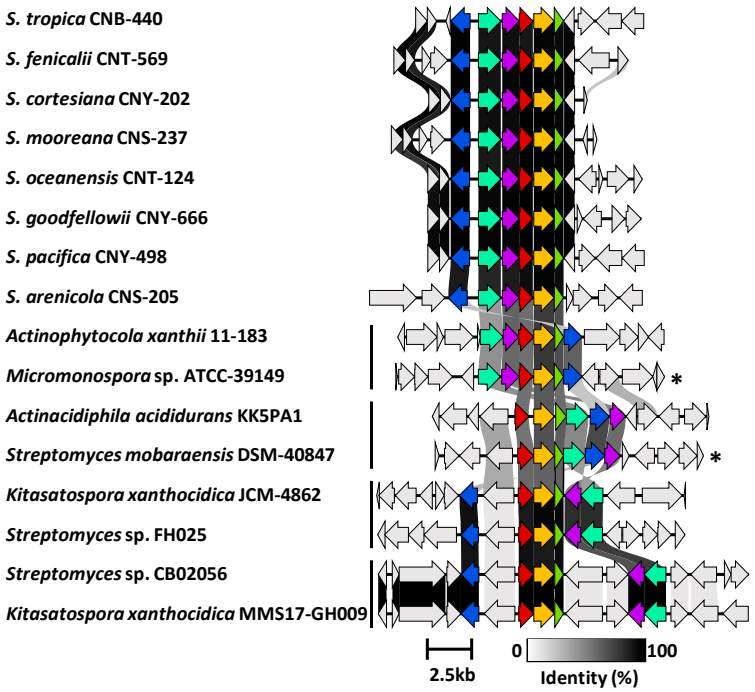

Figure 5. Synteny plot showing *ktm* and *ktm*-like biosynthetic gene clusters in *Salinispora* and diverse *Actinomycetota*. Representative *ktm* BGCs from eight *Salinispora* spp. are highly conserved across the genus (see Figure S17 for a full list). Four additional versions of the BGC (vertical bars) were observed among 28 *Actinomycetota* strains (see Figure S18 for a full list). Genes are colored as: *ktmA* (red), *ktmB* (yellow), *ktmC* (olive), *ktmD* (cyan), *ktmE* (blue), and *ktmF* (purple). Asterisks (*) denote experimentally validated *ktm* clusters outside of *Salinispora*.

We next used Cblaster to further assess the diversity and distribution of the *S. arenicola* CNY-498 *ktm* BGC within the NCBI genome database. We identified 28 non-*Salinispora* Actinomycetota that contain a BGC with homologs of *ktmA-F* (Figure S18), including *Micromonospora* sp. ATCC-39149 and *Streptomyces mobaraensis* NBRC 13,819 from which the *ktm* BGCs were heterologously expressed (Figure 1) [1]. These sequences could be grouped into four *ktm*-like BGC types based on gene synteny (Figure 5). While the products of two

of these have been experimentally validated, the other two could yield new ketomemicin or ketomethylene-containing pseudopeptide natural products.

2.4. Biological Activities of Ketomemicins

Due to their structural similarity to the arphamenines, which are known protease inhibitors [5,6], **1**–**3** were tested at 10 μM against a panel of eleven proteases of diverse origins, including humans (cathepsin B, D, L, aminopeptidase B, and human 20S proteasome), parasites (cruzain and *Trypanosoma brucei* cathepsin L), and viruses (SARS-CoV, SARS-CoV-2, and MERS-CoV main proteases, and papain-like protease) (Table 1). At these concentrations, ketomemicins **1**–**3** were not active against aminopeptidase B, which is the target of the arphamenines. The only activity detected was for compound **2**, which displayed moderate inhibition against the main proteases (M^{pro}) of SAR-CoV-1, SARS-CoV-2, and MERS-CoV as well as cruzain, while not being active against TbrCatL. Compounds **1**–**3** were also tested for antibacterial activity against *Escherichia coli* MG1655 and *Pseudomonas aeruginosa* and were inactive at the highest test concentration (32 μg/μL).

Table 1. Inhibitory activities of ketomemicins **1**–**3** (at 10 μM) against a panel of eleven proteases. Average percent inhibition is reported for the mean of two independent experiments each performed in triplicate. Errors are given as the ratio of the standard deviation to the square root of the number of measurements. Control inhibitors (highlighted in grey) were tested at 10 μM, except for nirmatrelvir (tested at 100 nM). Cat B: Cathepsin B; Cat D: cathepsin D; Cat L: cathepsin L; TbrCatL: *Trypanosoma brucei* cathepsin-L like; PL^{pro}: papain-like protease; h20S: human 20S proteasome.

Compound	Aminopeptidase B	Cat D	Cat B	Cat L	Cruzain	TbrCatL	PL^{pro}	SARS-CoV-2 M^{pro}	SARS-CoV M^{pro}	MERS-CoV M^{pro}	h20S ß1	h20S ß2	h20S ß5
1	2.2 ± 2	12 ± 3	2 ± 1	1 ± 1	13 ± 4	7 ± 4	1 ± 1	8 ± 5	2 ± 2	0.6 ± 1	5 ± 3	8 ± 2	1 ± 1
2	2.1 ± 2	1 ± 1	1 ± 1	0 ± 0	51 ± 4	10 ± 3	4 ± 3	43 ± 7	54 ± 8	51 ± 4	3 ± 2	3 ± 1	0 ± 0
3	1.7 ± 2	7 ± 2	3 ± 2	0 ± 0	1 ± 0.5	1 ± 1	7 ± 2	4 ± 2	1 ± 1	6 ± 3	1 ± 5	2.5 ± 3	0 ± 0
Bestatin	100 ± 0												
Pepstatin		100 ± 0											
E-64			96 ± 1	98 ± 1	98 ± 1	99 ± 1							
GRL0617							83 ± 2						
Nirmatrelvir								89 ± 2	98 ± 6	57 ± 1			
Salinosporamide A											100 ± 0	100 ± 0	66 ± 5

3. Conclusions

We present here the structures of newly identified ketomemicins from cultures of the marine actinomycete *Salinispora pacifica* CNY-498. Additionally, we analyzed the distribution of ketomemicins and the ketomemicin biosynthetic gene cluster (*ktm*) across a paired metabolomic and genomic dataset of 118 *Salinispora* strains. Beyond *Salinispora*, we identified two distinct ketomemicin-like BGCs that may encode yet-to-be-characterized variants within this natural product family. Finally, we evaluated the inhibitory activities of ketomemicins against a range of proteases.

4. Materials and Methods

4.1. General Experimental Procedures

Optical rotations were recorded on a Jasco P-2000 polarimeter (JASCO Analytical Instruments, Easton, MD, USA). UV spectra were measured on a Beckman-Coulter DU800 spectrophotometer (Beckman Coulter, Indianapolis, IN, USA). 1D and 2D NMR spectroscopic data were obtained on a JEOL 500 MHz (JEOL, Akishima, Tokyo, Japan) or a Bruker 600 MHz (Bruker Biospin, Billerica, MA, USA) NMR spectrometer. NMR chemical shifts were referenced to the residual solvent peaks (δH 3.31 and δC 49.15 for CD_3OD). High-resolution ESI-TOF mass spectrometric data were acquired on an Agilent

6530 (Agilent, Santa Clara, CA, USA) Accurate-Mass Q-TOF mass spectrometer coupled to an Agilent 1260 LC system (Agilent, Santa Clara, CA, USA).

4.2. Cultivation

A frozen stock of *Salinispora pacifica* CNY-498 was inoculated into 50 mL of medium A1 [1% potato starch, 0.4% yeast extract, and 0.2% peptone in 2.2% InstantOcean® (Marineland, Blacksburg, VA, USA)]. The seed culture was shaken at 200 rpm and 28 °C for seven days then used to inoculate 1 L of medium A1 in a 2.8 L Fernbach flask. This culture was similarly shaken at 200 rpm and 28 °C for eight days, after which 20 mL were inoculated into each of 18 × 2.8 L Fernbach flasks containing 1 L of medium A1FB [A1 supplemented with 0.01% potassium bromide and 0.03% iron (III) sulfate (5·H_2O)]. After eight days of shaking at 200 rpm and 28 °C, 25 g of sterile XAD-7 adsorbent resin was added to each flask. After two additional days of cultivation, the 18 L were filtered through cheesecloth to collect the resin (and some cell material), which were soaked in acetone (3 L) for 2 h with gentle agitation. The acetone extract was filtered through a cotton plug and concentrated via rotary evaporation. The resulting solution was partitioned in a separatory funnel between EtOAc and H_2O (1:1 mixture, 1 L total). The organic phase was collected, dried over anhydrous sodium sulfate, and concentrated via rotary evaporation to yield a red crude extract (500 mg).

4.3. Isolation of Ketomemicins

The organic extract was fractionated using C18 column flash chromatography (5g) and a six-step elution gradient from 100% H_2O (0.1% formic acid) to 100% MeCN (0.1% formic acid) to yield six fractions. Fraction 4 (60% MeCN, 18.8 mg) was concentrated, resuspended, and separated over HPLC [mobile phase: 70% MeCN in H_2O (0.1% formic acid) at 3 mL·min^{-1}; stationary phase: 5 µm, C18(2), 100 Å, 250 × 10 mm (Phenomenex, Luna) column] to yield subfractions A (2–4 min, 3.8 mg) and B (4–10 min, 11.9 mg). Subfraction A was further separated by HPLC [mobile phase: 30% MeCN in H_2O (0.1% formic acid) at 3 mL·min^{-1}; stationary phase: 5 µm, C18(2), 100 Å, 250 × 10 mm (Phenomenex, Luna) column] to yield ketomemicin C-318 (**1**, t_R = 14 min, 0.8 mg), ketomemicin C.332A (**2**, t_R = 20 min, 0.7 mg) and ketomemicin C.332B (**3**, t_R = 22 min, 0.5 mg).

Ketomemicin C-418 (**1**): $[\alpha]_{22}^{D}$ -41 (c 0.10, MeOH); UV/vis (MeOH) λ (log ε) 200 (3.23), 212 (3.01) nm; ^{1}H and 2D NMR, Table S1.

Ketomemicin C-432A (**2**): $[\alpha]_{22}^{D}$ -44 (c 0.10, MeOH); UV/vis (MeOH) λ (log ε) 200 (3.14), 212 (2.88) nm) nm; ^{1}H and 2D NMR, Table S2.

Ketomemicin C-432B (**3**): $[\alpha]_{22}^{D}$ -43 (c 0.10, MeOH); UV/vis (MeOH) λ (log ε) 200 (3.03), 212 (2.74) nm) nm; ^{1}H and 2D NMR, Table S3.

Supplementary Materials: The following supporting information can be downloaded at: https://www.mdpi.com/article/10.3390/md23030126/s1, Figures S1–S18 and Tables S1–S8: ^{1}H, COSY, HSQC, and HMBC NMR spectra and MS spectra for **1**–**3**, calculated ^{1}H and ^{13}C NMR chemical shifts for diastereomers of **1**, and distribution of ketomemicins and *ktm* BGC in *Salinispora* strains.

Author Contributions: Conceptualization, G.C.-F., D.G.G.-M. and P.R.J.; methodology, G.C.-F., D.G.G.-M., W.G. and E.B.D.S.; formal analysis, G.C.-F., D.G.G.-M., E.B.D.S., W.G., A.R., M.S.M.S. and T.H.M.F.; writing—original draft preparation, G.C.-F., D.G.G.-M. and P.R.J.; writing—review and editing, all authors; supervision, D.J.T., A.J.O. and P.R.J.; funding acquisition, D.J.T., A.J.O. and P.R.J. All authors have read and agreed to the published version of the manuscript.

Funding: This research was funded by the National Institutes of Health, grant number R01GM085770, to P.R.J. G.C.-F is a San Diego IRACDA Scholar supported by the National Institutes of Health/NIGMS K12 GM068524 Award. A high-resolution LC-MS instrument was provided by the National Institutes of Health, grant number S10 OD0106400.

Institutional Review Board Statement: Not applicable.

Data Availability Statement: NMR data for **1**–**3** has been deposited in the Natural Products Magnetic Resonance Database (NP-IDs: NP0350792, NP0350793, and NP0350794) (www.np-mrd.org). MS^2 data for **1** was deposited in the Global Natural Products Social Molecular Networking (GNPS) library (Acc: CCMSLIB00011436670) (www.gnps.ucsd.edu). Other original contributions presented in this study are included in the article/Supplementary Material. Further inquiries can be directed to the corresponding author.

Acknowledgments: We thank B. Duggan from the UCSD SSPPS NMR Facility and A. Mrse from the UCSD Department of Chemistry and Biochemistry for assistance with NMR experiments, Y. Su from the UCSD Molecular Mass Spectrometry Facility for HRMS measurements, and P. Fajtova from UCSD Skaggs School of Pharmacy for assistance with the proteasome assay. We thank the CAPES Foundation, grant numbers 88887.595578/2020-00 and 88887.684031/2022-00 for funding to M.S.M.S. Computational support from the NSF ACCESS program is gratefully acknowledged.

Conflicts of Interest: The authors declare no conflicts of interest.

References

1. Ogasawara, Y.; Kawata, J.; Noike, M.; Satoh, Y.; Furihata, K.; Dairi, T. Exploring peptide ligase orthologs in actinobacteria—Discovery of pseudopeptide natural products, ketomemicins. *ACS Chem. Biol.* **2016**, *11*, 1686–1692. [CrossRef]
2. Ogasawara, Y.; Fujimori, M.; Kawata, J.; Dairi, T. Characterization of three amidinotransferases involved in the biosynthesis of ketomemicins. *Bioorg. Med. Chem. Lett.* **2016**, *26*, 3662–3664. [CrossRef] [PubMed]
3. Kawata, J.; Naoe, T.; Ogasawara, Y.; Dairi, T. Biosynthesis of the carbonylmethylene structure found in the ketomemicin class of pseudotripeptides. *Angew. Chem. Int. Ed.* **2017**, *56*, 2026–2029. [CrossRef]
4. Jensen, P.R.; Moore, B.S.; Fenical, W. The marine actinomycete genus *Salinispora*: A model organism for secondary metabolite discovery. *Nat. Prod. Rep.* **2015**, *32*, 738–751. [CrossRef] [PubMed]
5. Ohuchi, S.; Suda, H.; Naganawa, H.; Takita, T.; Aoyagi, T.; Umezawa, H.; Nakamura, H.; Iitaka, Y. The structure of arphamenines A and B. *J. Antibiot.* **1983**, *36*, 1576–1580. [CrossRef] [PubMed]
6. Umezawa, H.; Aoyagi, T.; Ohuchi, S.; Okuyama, A.; Suda, H.; Takita, T.; Hamada, M.; Takeuchi, T. Arphamenines A and B, new inhibitors of aminopeptidase B, produced by bacteria. *J. Antibiot.* **1983**, *36*, 1572–1575. [CrossRef]
7. Zalman, L.S.; Brothers, M.A.; Dragovich, P.S.; Zhou, R.; Prins, T.J.; Worland, S.T.; Patick, A.K. Inhibition of human rhinovirus-induced cytokine production by AG7088, a human rhinovirus 3C protease inhibitor. *Antimicrob. Agents Chemother.* **2000**, *44*, 1236–1241. [CrossRef]
8. Kaysser, L. Built to bind: Biosynthetic strategies for the formation of small-molecule protease inhibitors. *Nat. Prod. Rep.* **2019**, *36*, 1654–1686. [CrossRef]
9. Armirotti, A.; Millo, E.; Damonte, G. How to discriminate between leucine and isoleucine by low energy ESI-TRAP MSn. *J. Am. Soc. Mass Spectrom.* **2007**, *18*, 57–63. [CrossRef]
10. Lodewyk, M.W.; Siebert, M.R.; Tantillo, D.J. Computational prediction of NMR chemical shifts. *Chem. Rev.* **2012**, *112*, 1839–1862. [CrossRef]
11. Pracht, P.; Bohle, F.; Grimme, S. Automated exploration of the low-energy chemical space with fast quantum chemical methods. *Phys. Chem. Chem. Phys.* **2020**, *22*, 7169–7192. [CrossRef] [PubMed]
12. Frisch, M.J.; Trucks, G.W.; Schlegel, H.B.; Scuseria, G.E.; Robb, M.A.; Cheeseman, J.R.; Scalmani, G.; Barone, V.; Petersson, G.A.; Nakatsuji, H.; et al. *Gaussian 16, Revision C.01*; Gaussian, Inc.: Wallingford, CT, USA, 2016.
13. Lee, C.; Yang, W.; Parr, R.G. Development of the Colle-Salvetti correlation-energy formula into a functional of the electron density. *Phys. Rev. B* **1988**, *37*, 785–789. [CrossRef]
14. Grimme, S.; Ehrlich, S.; Goerigk, L. Effect of the damping function in dispersion-corrected density functional theory. *J. Comput. Chem.* **2011**, *32*, 1456–1465. [CrossRef] [PubMed]
15. Clark, T.; Chandrasekhar, J.; Spitznagel, G.W.; Schleyer, P.V.R. Efficient diffuse function-augmented basis sets for anion calculations. III. The 3-21+G basis set for first-row elements, Li–F. *J. Comput. Chem.* **1983**, *4*, 294–301. [CrossRef]
16. Pascual-Ahuir, J.L.; Silla, E.; Tuñon, I. GEPOL: An improved description of molecular surfaces. III. A new algorithm for the computation of a solvent-excluding surface. *J. Comput. Chem.* **1994**, *15*, 1127–1138. [CrossRef]
17. Adamo, C.; Barone, V. Exchange functionals with improved long-range behavior and adiabatic connection methods without adjustable parameters: The mPW and mPW1PW models. *J. Chem. Phys.* **1998**, *108*, 664–675. [CrossRef]
18. Krishnan, R.; Binkley, J.S.; Seeger, R.; Pople, J.A. Self-consistent molecular orbital methods. XX. A basis set for correlated wave functions. *J. Chem. Phys.* **1980**, *72*, 650–654. [CrossRef]

19. Willoughby, P.H.; Jansma, M.J.; Hoye, T.R. Addendum: A guide to small-molecule structure assignment through computation of (1H and 13C) NMR chemical shifts. *Nat. Protoc.* **2020**, *15*, 2277. [CrossRef]
20. Zanardi, M.M.; Sarotti, A.M. Sensitivity analysis of DP4+ with the probability distribution terms: Development of a universal and customizable method. *J. Org. Chem.* **2021**, *86*, 8544–8548. [CrossRef]
21. Wang, M.; Carver, J.J.; Phelan, V.V.; Sanchez, L.M.; Garg, N.; Peng, Y.; Nguyen, D.D.; Watrous, J.; Kapono, C.A.; Luzzatto-Knaan, T.; et al. Sharing and community curation of mass spectrometry data with Global Natural Products Social Molecular Networking. *Nat. Biotechnol.* **2016**, *34*, 828–837. [CrossRef]
22. Duncan, K.R.; Crüsemann, M.; Lechner, A.; Sarkar, A.; Li, J.; Ziemert, N.; Wang, M.; Bandeira, N.; Moore, B.S.; Dorrestein, P.C.; et al. Molecular Networking and Pattern-Based Genome Mining Improves Discovery of Biosynthetic Gene Clusters and their Products from *Salinispora* Species. *Chem. Biol.* **2015**, *22*, 460–471. [CrossRef] [PubMed]
23. Crüsemann, M.; O'Neill, E.C.; Larson, C.B.; Melnik, A.V.; Floros, D.J.; da Silva, R.R.; Jensen, P.R.; Dorrestein, P.C.; Moore, B.S. Prioritizing Natural Product Diversity in a Collection of 146 Bacterial Strains Based on Growth and Extraction Protocols. *J. Nat. Prod.* **2017**, *80*, 588–597. [CrossRef] [PubMed]
24. Chase, A.B.; Sweeney, D.; Muskat, M.N.; Guillén-Matus, D.G.; Jensen, P.R. Vertical Inheritance Facilitates Interspecies Diversification in Biosynthetic Gene Clusters and Specialized Metabolites. *mBio* **2021**, *12*, e02700-21. [CrossRef]
25. Pluskal, T.; Castillo, S.; Villar-Briones, A.; Oresic, M. MZmine 2: Modular framework for processing, visualizing, and analyzing mass spectrometry-based molecular profile data. *BMC Bioinform.* **2010**, *11*, 395. [CrossRef] [PubMed]
26. Román-Ponce, B.; Millán-Aguiñaga, N.; Guillen-Matus, D.; Chase, A.B.; Ginigini, J.G.M.; Soapi, K.; Feussner, K.D.; Jensen, P.R.; Trujillo, M.E. Six novel species of the obligate marine actinobacterium *Salinispora*, *S. cortesiana* sp. nov., *S. fenicalii* sp. nov., *S. goodfellowii* sp. nov., *S. mooreana* sp. nov., *S. oceanensis* sp. nov., and *S. vitie* sp. nov. *Int. J. Syst. Evol. Microbiol.* **2020**, *70*, 4668–4682. [CrossRef]
27. Blin, K.; Shaw, S.; Kloosterman, A.M.; Charlop-Powers, Z.; van Wezel, G.P.; Medema, M.H.; Weber, T. antiSMASH 6.0: Improving cluster detection and comparison capabilities. *Nucleic Acids Res.* **2021**, *49*, W29–W35. [CrossRef]
28. Gilchrist, C.L.M.; Booth, T.J.; van Wersch, B.; van Grieken, L.; Medema, M.H.; Chooi, Y.-H. cblaster: A remote search tool for rapid identification and visualization of homologous gene clusters. *Bioinform. Adv.* **2021**, *1*, vbab016. [CrossRef]
29. Bruns, H.; Crüsemann, M.; Letzel, A.-C.; Alanjary, M.; McInerney, J.O.; Jensen, P.R.; Schulz, S.; Moore, B.S.; Ziemert, N. Function-related replacement of bacterial siderophore pathways. *ISME J.* **2018**, *12*, 320–329. [CrossRef]
30. Gilchrist, C.L.M.; Chooi, Y.-H. clinker & clustermap.js: Automatic generation of gene cluster comparison figures. *Bioinformatics* **2021**, *37*, 2473–2475. [CrossRef]
31. Creamer, K.E.; Kudo, Y.; Moore, B.S.; Jensen, P.R. Phylogenetic analysis of the *salinipostin* γ-butyrolactone gene cluster uncovers new potential for bacterial signalling-molecule diversity. *Microb. Genom.* **2021**, *7*, e000568. [CrossRef]